Pergamon

Int. J. Heat Mass Transfer. Vol. 38, No. 11, pp. 2001–2010, 1995

0017-9310/95 $9.50+0.00

0017-9310(94)00316-5

Transient conduction in eccentrically hollow cylinders

MAGED A. I. EL-SHAARAWI and ESMAIL MOKHEIMER

Mechanical Engineering Department, King Fahd University of Petroleum and Minerals, Dhahran 31261, Saudi Arabia

(*Received* 13 *October* 1993 *and in final form* 27 *September* 1994)

Abstract—Transient heat conduction with uniform rate of internal heat generation has been numerically investigated in infinitely long eccentrically hollow cylinders. Two combinations of boundary conditions of the first and second kinds have been considered. The first of these combinations corresponds to the case of one surface being heated isothermally while the opposite surface is maintained at ambient temperature. The second combination of boundary conditions is with one surface maintained isothermal while the opposite surface is adiabatic. Results are presented for a radius ratio 0.5 with dimensionless eccentricities ranging from 0.1 to 0.8 and various values of internal heat generation.

INTRODUCTION

Heat generated in underground electric cable systems due to conductor losses and magnetic effects can be transferred to the earth. However, the rate of heat dissipation from a cable and hence its insulation temperature limit the electrical transmission capacity of underground cable system (Abdulhadi and Chato [1]). To increase the current carrying capacity, cooling techniques by an annular gap of gas or oil may be proposed. Thermal expansion of the cable inside the fluid gap changes the radial position of the inner cable relative to its outer housing wall and therefore eccentric annular configurations can exist. The horizontal annular configuration can also be found in the field of solar energy utilization. In the so-called parabolic-cylindrical solar collector, a circular receiver tube, with a suitable selective coating, is enclosed by a concentric glass envelope and situated along the focal line of a parabolic trough reflector. Eccentricity between the receiver tube and its glass envelope would indeed affect the resistance to heat transfer in this system. On the other hand, heat transfer in vertical annular channels can occur in many engineering applications (El-Shaarawi and Sarhan [2] and El-Shaarawi and Al-Nimr [3]). In practical situations the manufacturing tolerances and operating conditions can introduce eccentricities in nominally concentric annuli.

Prior to the onset of free convection in an annular channel the conduction mode is the prevailing heat transfer mode, particularly when the temperature is low and radiation is negligible. Heat conduction and heat storage capacity in eccentric configurations may also be important in cases of eccentrically drilled tubes or hollow shafts or eccentric insulations.

Since an annulus has two boundary surfaces on which thermal conditions may be independently imposed, there is a large number of conduction heat transfer problems of significant interest. However, with some usual assumptions [4] the energy equation becomes linear and homogeneous and consequently the superposition technique can be utilized provided that the boundary conditions are also linear. With the application of such a mathematical technique, a solution (temperature field) satisfying arbitrary boundary conditions could be determined by simply adding multiples of solutions (temperature fields) satisfying certain simple boundary conditions. For example, on each of the two boundary surfaces, one of the following three linear boundary conditions is usually employed. The temperature may be constant, or the temperature gradient (normal to the boundary) may be constant (i.e. constant heat flux when the thermal conductivity k is constant), or there may be heat exchange by convection with an environment at a constant ambient temperature according to Newton's law of cooling (i.e. heat transfer is linearly proportional to the difference between the temperature of the boundary and that of the environment). These simple-linear boundary conditions are usually referred to as the boundary condition of the first kind, the second kind and the third kind, respectively [4]. Thus, for an annulus, there are nine heat conduction problems corresponding to the possible nine combinations of the aforesaid thermal conditions on the two surface boundaries. Ozisik [4] presented exact solutions for these nine heat conduction problems in concentric hollow cylinders when the boundary conditions of the first, second, and third kind are homogeneous. However, since the two cylindrical boundaries of an annulus have unequal areas these nine combinations of the three simple-linear boundary conditions can indeed give 18 different physical situations when the asymmetric thermal conditions are interchanged on the inner and outer boundaries in each case.

NOMENCLATURE

A	constant of integration in equations (12) and (14), given in Table 1
a	constant in bipolar transformation equations (location of the positive pole of the bipolar coordinate system), equal $r_i \sinh \eta_i$ or $r_o \sinh \eta_o$
B	constant of integration in equations (12) and (14), given in Table 1
C	constant of integration in equations (12) and (14), given in Table 1
c	specific heat of the solid material
C^*	constant equal to $H^2(\cosh \eta - \cos \xi)^2$ $Q = [(\sinh \eta_o)/(2\{1-N\})]^2 Q$
D	equivalent diameter of annulus, $2(r_o - r_i)$
D^*	constant of integration in equations (12) and (14), given in Table 1
E	dimensionless eccentricity or dimensionless center-to-center distance, $e/(r_o - r_i)$
e	eccentricity (distance between the two centers of the circular boundaries of the solid), $a(\coth \eta_o - \coth \eta_i)$
H	dimensionless transformation factor, $h/D = \sinh \eta_o/[2(1-N)(\cosh \eta - \cos \xi)]$
h	coordinate transformation scale factor, $a/(\cosh \eta - \cos \xi)$
k	thermal conductivity of the solid
m	number of steps of the numerical mesh network in the ξ-direction
N	annulus radius ratio, $r_i/r_o = \sinh \eta_o/\sinh \eta_i$
n	number of steps of the numerical mesh network in the η-direction or infinite-series summation parameter in steady-state solution
Q	dimensionless rate of internal heat generation $q D^2/k(T_w - T_o)$
q	rate of internal heat generation per unit volume of solid
r_i	inner radius of the annular solid
r_o	outer radius of the annular solid
T	temperature
T_o	ambient or initial temperature
T_w	isothermal temperature of heat-transfer boundary
t	dimensionless time, $\alpha\tau/D^2$
x	first Cartesian coordinate
y	second Cartesian coordinate
z	axial coordinate (third Cartesian coordinate).

Greek symbols

α	thermal diffusivity of solid, $k/\rho c$
θ	dimensionless temperature, $(T-T_o)/(T_w-T_o)$
θ_c	complementary solution of the steady-state energy equation
θ_p	particular solution of the steady-state energy equation
θ_s	general solution of the steady-state energy equation
η	first bipolar coordinate
ξ	second bipolar coordinate
ν	third bipolar coordinate
ρ	density of solid
τ	time.

Subscripts

c	complementary part of steady-state solution
i	on the inner surface
o	on the outer surface or initial (ambient) value
p	particular integral part of steady-state solution
s	steady-state conditions
w	on the heat-transfer boundary.

The above discussion concerning superposition of solutions corresponding to simple boundary conditions is also applicable to fully developed forced or natural convection in annular passages. However, the boundary condition of the third kind is meaningless in such convection problems. Therefore, Reynolds *et al.* [5] completely solved the problem of heat transfer to fully developed laminar flow in concentric annuli by defining only four fundamental boundary conditions. These fundamental boundary conditions are combinations of the aforesaid boundary conditions of the first and second kind when applied on each of the two boundaries of an annulus. The fundamental boundary conditions of the first type correspond to a prescribed isothermal temperature at one wall while the opposite wall is kept isothermal at the inlet fluid temperature. The second fundamental boundary conditions are when one wall is maintained at uniform heat flux (constant temperature gradient) and the opposite wall is adiabatic. The fundamental boundary conditions of the third kind are obtained by keeping one of the walls isothermal and the opposite wall adiabatic. The fourth fundamental boundary conditions correspond to one wall maintained at uniform heat flux while the opposite wall is kept isothermal at the inlet fluid temperature. Exact fundamental solutions corresponding to these four fundamental boundary conditions have been obtained in concentric annuli for fully developed forced convection by Lundberg *et al.* [6] and for fully developed natural convection by El-Shaarawi and Al-

Nimr [3]. Trombetta [7] obtained approximate solutions for fully developed forced convection in eccentric annuli under the fundamental boundary conditions of the first, second and fourth types.

Exact solutions for conduction heat transfer in cylinders with an eccentric bore (eccentric annuli) and uniform rate of internal heat generation are available in the literature only for the steady-state case. El-Saden [8] obtained an exact solution for the steady conduction in an infinitely long, eccentrically hollow cylinder with uniform rate of internal heat generation when the boundary surfaces are maintained at constant but different temperatures. Rather than using bipolar coordinates, Eckert and Drake [9] analyzed and obtained an approximate solution for the same problem by the superposition of infinite line heat source and sink solutions. DeFelice and Bau [10] presented an exact solution for the steady case with no internal heat generation when boundary conditions of the third kind (convective boundary conditions) are imposed on both surfaces.

The problem of heat conduction in a homogeneous semi-infinite soil surrounding a cylindrical heat source buried at a specified depth below an isothermal horizontal surface is a special case of the above mentioned conduction problem in eccentric annuli. Approximate solutions, by the superposition of infinite line heat source and sink solutions, for this special problem with an isothermal heat source were obtained under the transient and steady-state conditions by Ioffe [11] and Eckert and Drake [9], respectively. Exact steady solutions by the use of bipolar (bicylindrical) coordinates were obtained by Thiyagarajan and Yovanovich [12] for the constant heat flux boundary condition and by Bau and Sadhal [13] for the case of a constant convective heat transfer coefficient and the case of a linear temperature variation along the heat source surface. Using bipolar coordinates, Martin and Sadhal [14] determined the upper and lower bounds on the transient temperature distribution and approximate solutions for engineering estimates for the case with a convection boundary condition on the cylindrical heat source.

A careful search of the literature failed to disclose any prior work on the problem of transient conduction heat transfer in eccentrically hollow cylinders with or without internal heat generation. This motivated the present work which addresses the transient case numerically and the steady-state case analytically (using the closed-form steady solution of El-Saden [8]). Moreover, the importance of the conduction problem as the limiting case of convection heat transfer in eccentric annular passages guided the selection of the investigated thermal boundary conditions. In this paper two combinations of boundary conditions of the first and second kinds have been imposed on the two surfaces of the annulus. These two combinations correspond to the fundamental boundary conditions of the first and third types, according to the definitions of fundamental boundary conditions by Reynolds *et al.* [5].

PROBLEM FORMULATION AND BOUNDARY CONDITIONS

The geometry of the problem under consideration is an infinitely long, eccentrically hollow cylinder for which a two-dimensional cross-section is shown in Fig. 1(a). The eccentric annular solid material is assumed to have constant physical properties and uniform internal heat generation per unit volume. For any prescribed thermal conditions on the two circular boundaries of this geometry and an initial condition, the unsteady heat conduction in the solid eccentric annulus is governed, in the Cartesian (x–y) plane, by the following two dimensional transient energy equation

$$\frac{\partial^2 T}{\partial x^2}+\frac{\partial^2 T}{\partial y^2}+\frac{q}{k}=\frac{1}{\alpha}\frac{\partial T}{\partial \tau}. \tag{1}$$

The geometry under consideration can easily be described by the more convenient bipolar coordinate system (η, ξ and γ) shown in Fig. 1(b). In this system, constant η and ξ are two sets of orthogonal circles in the physical (x–y) plane. The third coordinate (γ-axis) is perpendicular to the plane of the paper. The two surfaces of the solid annulus under consideration are represented by constant values of η. The transformation from rectangular to bipolar coordinates is given by the following equations [15]

$$x=\frac{a\sinh\eta}{\cosh\eta-\cos\xi} \tag{2}$$

$$y=\frac{a\sin\xi}{\cosh\eta-\cos\xi} \tag{3}$$

and

$$z=\gamma. \tag{4}$$

In the above equations, "a" is a constant ($a=r_i\sinh\eta_i=r_o\sinh\eta_o$). The first set of circles, $-\infty<\eta<\infty$, have radii equal ($a\operatorname{csch}\eta$) and their centers are on the x-axis at ($a\coth\eta$, 0). Thus the eccentricity, e, is equal to $a(\coth\eta_o-\coth\eta_i)$. The second set of circles, $0\leqslant\xi\leqslant 2\pi$, have radii equal ($a\csc\xi$), their centers are on the y-axis at (0, $a\cot\xi$) and all pass by the poles of the system at (a,0) and ($-a$,0). The transformed geometry in the complex η–ξ plane is, as shown in Fig. 1(c), a slab of length ($\eta_i-\eta_o$) and width equal to the limits of ξ, that is 2π.

Using the transformation equations (2)–(4), it may be shown that the governing equation (1) is transformed in the η–ξ coordinate system into the following equation

$$\frac{\partial^2 T}{\partial \eta^2}+\frac{\partial^2 T}{\partial \xi^2}+h^2\frac{q}{k}=\frac{h^2}{\alpha}\frac{\partial T}{\partial \tau}. \tag{5}$$

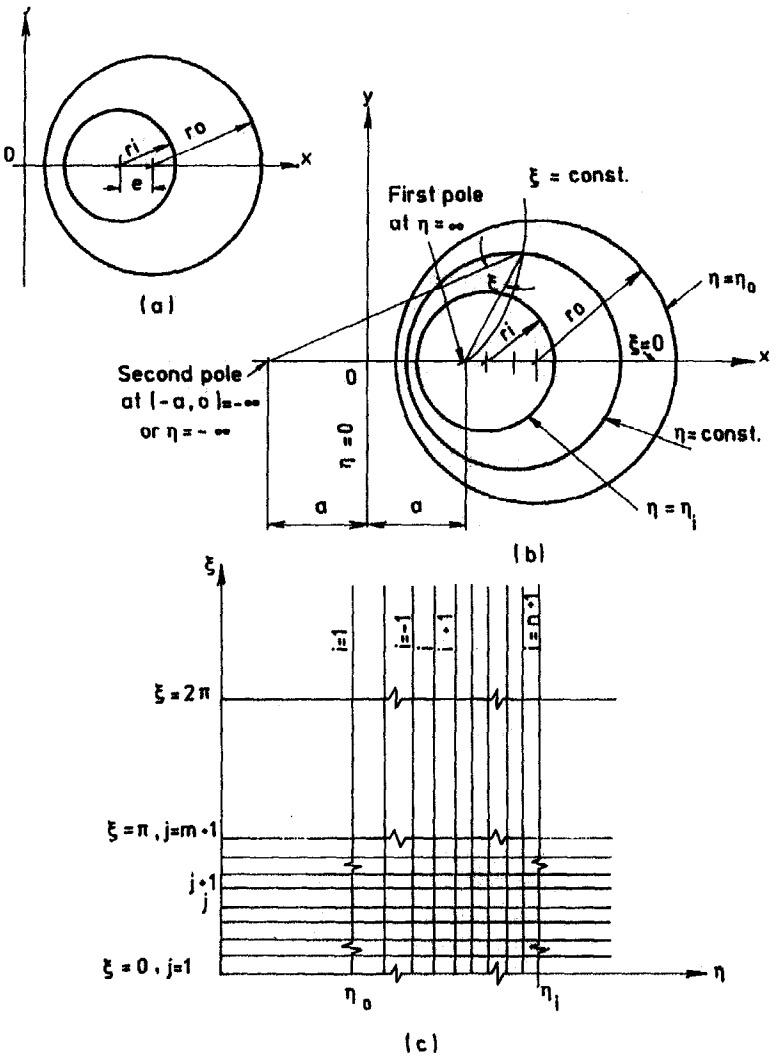

Fig. 1. (a) Two-dimensional cross-section of the geometry under consideration; (b) bipolar coordinate system; (c) transformed geometry in η–ξ plane and the numerical mesh network.

In the above equation h is the coordinate transformation scale factor $[h = a/(\cosh\eta - \cos\xi)]$. The equation and the boundary conditions are linear in the dependent variable (T) and hence fundamental solutions can be utilized to obtain more general solutions. It is to be noted that in each of the previously specified four fundamental boundary conditions there is one boundary maintained either adiabatic $(\partial T/\partial\eta = 0)$ or at ambient temperature T_o. The boundary opposite to that maintained adiabatic or at T_o is called the heat transfer boundary (El-Shaarawi and Al-Nimr [3]). Thus, as the heat transfer boundary might be the inner or the outer surface, there are eight fundamental solutions that can be considered. For each of the previously mentioned four fundamental boundary conditions there are two possible cases that can be considered, namely, case I, in which the heat transfer boundary is at the inner surface and case O, in which the heat transfer boundary is at the outer surface. Thus each of the eight cases that can be considered under the previously defined four fundamental boundary conditions may be designated by a number (1, 2, 3 or 4) and a letter (either I or O). The number would refer to the fundamental boundary conditions under consideration (e.g. 1 refers to fundamental boundary conditions of first type) and the letter refers to the heat transfer boundary. Thus, case (1.I) refers to a case under fundamental boundary conditions of the first type with the inner surface being the heat transfer boundary. Similarly, case (3.O) refers to a case under fundamental boundary conditions of the third kind with the outer surface being the heat transfer boundary, and so on. In the present work, only the following cases have been considered: (1.I), (1.O), (3.I) and (3.O).

Using the dimensionless parameters given in the

nomenclature the governing equation (5) can be written, for all the cases under consideration, in the following non-dimensional form

$$\frac{\partial^2\theta}{\partial\eta^2}+\frac{\partial^2\theta}{\partial\xi^2}+H^2Q=H^2\frac{\partial\theta}{\partial t}. \quad (6)$$

Due to symmetry, the following two boundary conditions with respect to ξ are applicable

$$\text{for } \xi=0 \text{ or } \pi: \partial\theta/\partial\xi=0. \quad (7)$$

On the other hand, in all the cases considered the solid is initially ($t\leqslant 0$) at ambient temperature, i.e.

$$\text{for } t\leqslant 0: \theta=0. \quad (8)$$

Then (when $t>0$) the heat is internally generated in the solid and simultaneously one of its surfaces is isothermally heated to T_w while the other surface is kept either at the initial ambient temperature T_o or adiabatic. Thus the two boundary conditions with respect to η for the four cases considered are as follows

Case	1.I	1.O	3.I	3.O
B.C. on $\eta=\eta_i$	$\theta=1$	$\theta=0$	$\theta=1$	$\frac{\partial\theta}{\partial\eta}=0$
B.C. on $\eta=\eta_o$	$\theta=0$	$\theta=1$	$\frac{\partial\theta}{\partial\eta}=0$	$\theta=1$. (9)

ANALYTICAL STEADY-STATE SOLUTIONS

Under steady-state conditions equation (6) reduces to

$$\frac{\partial^2\theta}{\partial\eta^2}+\frac{\partial^2\theta}{\partial\xi^2}=-H^2Q=\frac{-C^*}{(\cosh\eta-\cos\xi)^2}. \quad (10)$$

Such steady-state conditions are achieved at considerably large values of time, i.e. the solution to the transient problem should asymptotically approach its corresponding steady-state value. Thus, steady-state analytical solutions can provide a check on the adequacy of the present transient numerical results.

The general solution of the steady-state equation (10) is given by El-Saden [8], as

$$\theta_s(\eta,\xi)=\theta_c+\theta_p \quad (11)$$

where the complementary part of the solution, after applying the boundary conditions (7), is

$$\theta_c=A\eta+B+\sum_{n=1}^{\infty}(Ce^{n\eta}+D^*e^{-n\eta})\cos n\xi \quad (12)$$

and the particular integral part of the solution, which is due to the internal heat generation, is

$$\theta_p=-\frac{C^*}{2}\frac{\cosh\eta}{\cosh\eta-\cos\xi}$$

$$=-\frac{C^*}{2}\coth\eta-C^*\sum_{n=1}^{\infty}\coth\eta\,e^{-n\eta}\cos n\xi. \quad (13)$$

The series part on the right-hand side of equation (12) or (13) is due to the eccentricity and the general solution (11) can now be written in the following form

$$\theta_s=A\eta+B-\frac{C^*}{2}\coth\eta+\sum_{n=1}^{\infty}\cos n\xi$$

$$\times[Ce^{n\eta}+(D^*-C^*\coth\eta)e^{-n\eta}]. \quad (14)$$

It is worth mentioning that the right-hand side of equation (13) was given by El-Saden [8]; it can be obtained by finding a Fourier-cosine expansion of the even function $[1/(\cosh\eta-\cos\xi)]$ as shown in [16].

Applying the boundary conditions the constants A, B, C and D^* in equation (14) are obtained for the considered cases as given in Table 1. It is worth noting that the values of these constants for cases (1.I) and (1.O) are given in Table 1 for the sake of completeness. These were obtained before by El-Saden, but in terms of two different but constant dimensional values of temperatures on the boundary surfaces.

NUMERICAL METHOD OF SOLUTION

Equation (6) is very difficult to solve exactly since H is a function of η and ξ; hence we resort to numerical solution. Due to symmetry equation (6) needs to be solved for $0\leqslant\xi\leqslant\pi$, i.e. in only half the slab shown in Fig. 1(c). Figure 1(c) shows the numerical grid in the η–ξ plane where the independent variable θ is computed, for a given time t, at the intersections of the grid lines and (i, j) is a typical mesh point. Mesh points are numbered consecutively; i is progressing in the η-direction with $i=1,2,3,\ldots,n+1$ from the outer surface and j is progressing in the ξ-direction with $j=1,2,3,\ldots,m+1$ from the wide side of the annulus (at $\xi=0$).

Using the traditional alternating-direction implicit (ADI) finite-difference scheme we faced difficulties in obtaining convergent numerical solutions. On the other hand, the following finite-difference scheme has proved to be successful for all values of dimensionless eccentricity (E).

$$\frac{\theta_{i-1,j}-2\theta_{i,j}+\theta_{i+1,j}}{(\Delta\eta)^2}+\frac{\theta^*_{i,j-1}-2\theta^*_{i,j}+\theta^*_{i,j+1}}{(\Delta\xi)^2}$$

$$+H^2_{i,j}Q=H^2_{i,j}\frac{\theta_{i,j}-\theta^*_{i,j}}{\Delta\tau}, \quad (15)$$

where the asterisk (*) superscript denotes the previous time step and hence the superscripted θs are known.

The two boundary conditions given by equation (7) can be written, using backward and forward finite differences, respectively, as

$$\theta_{i,1}=\theta_{i,2} \quad (16)$$

and

$$\theta_{i,m+1}=\theta_{i,m}. \quad (17)$$

Similarly, the boundary conditions (9) on the inner

Table 1. Constants of equation (14) for various cases investigated

Case	A	B	C	D^*
1.I	$\dfrac{\frac{C^*}{2}(\coth\eta_i-\coth\eta_o)+1}{\eta_i-\eta_o}$	$\dfrac{\frac{C^*}{2}(\eta_i\coth\eta_o-\eta_o\coth\eta_i)-\eta_o}{\eta_i-\eta_o}$	$\dfrac{C^*(\coth\eta_o-\coth\eta_i)}{e^{2n\eta_o}-e^{2n\eta_i}}$	$\dfrac{C^*(e^{2n\eta_i}\coth\eta_o-e^{2n\eta_i}\coth\eta_i)}{e^{2n\eta_i}-e^{2n\eta_o}}$
1.O	$\dfrac{\frac{C^*}{2}(\coth\eta_i-\coth\eta_o)-1}{\eta_i-\eta_o}$	$\dfrac{\frac{C^*}{2}(\eta_i\coth\eta_o-\eta_o\coth\eta_i)+\eta_i}{\eta_i-\eta_o}$	Same as above	Same as above
3.I	$\dfrac{-C^*}{2\sinh^2\eta_o}$	$1+\dfrac{C^*\coth\eta_i}{2}+\dfrac{C^*\eta_i}{2\sinh^2\eta_o}$	$\dfrac{C^*\left[\coth\eta_i-\coth\eta_o-\left(\frac{1}{n\sinh^2\eta_o}\right)\right]}{e^{2n\eta_i}+e^{2n\eta_o}}$	$\dfrac{C^*\left[e^{2n\eta_o}\coth\eta_i+e^{2n\eta_i}\coth\eta_o+\left(\frac{e^{2n\eta_i}}{n\sinh^2\eta_i}\right)\right]}{e^{2n\eta_i}+e^{2n\eta_o}}$
3.O	$\dfrac{-C^*}{2\sinh^2\eta_i}$	$1+\dfrac{C^*\coth\eta_o}{2}+\dfrac{C^*\eta_o}{2\sinh^2\eta_i}$	$\dfrac{C^*\left[\coth\eta_o-\coth\eta_i-\left(\frac{1}{n\sinh^2\eta_i}\right)\right]}{e^{2n\eta_i}+e^{2n\eta_o}}$	$\dfrac{C^*\left[e^{2n\eta_i}\coth\eta_o+e^{2n\eta_o}\coth\eta_i+\left(\frac{e^{2n\eta_o}}{n\sinh^2\eta_i}\right)\right]}{e^{2n\eta_i}+e^{2n\eta_o}}$

and outer surfaces in cases 3.I and 3.O, respectively, can be rewritten as

$$\theta_{1,j}=\theta_{2,j} \tag{18}$$

and

$$\theta_{n+1,j}=\theta_{n,j}. \tag{19}$$

The problem under consideration is governed by three controlling parameters, namely, the annulus radius ratio (N), the dimensionless eccentricity (E) and the dimensionless internal heat generation (Q). A numerical solution can be obtained by first selecting values of these controlling parameters. In the present work computations were carried out in an annulus of radius ratio 0.5 for various selected values of E and Q. The radius ratio 0.5 was chosen since it represents a typical annular geometry with its value of N far enough from unity ($N=1$) which represents the case of a slab bounded by two parallel-plate surfaces. Knowing the radius ratio (N) and the eccentricity (E), the values of η for the inner and outer surfaces are computed by the following two equations respectively

$$\eta_i=\log_e\left[\frac{N(1+E^2)+(1-E^2)}{2NE}+\sqrt{\left(\frac{N(1+E^2)+(1-E^2)}{2NE}\right)^2-1}\right]$$

$$\eta_o=\log_e\left[\frac{N(1-E^2)+(1+E^2)}{2E}+\sqrt{\left(\frac{N(1-E^2)+(1+E^2)}{2E}\right)^2-1}\right].$$

Having computed η_i and η_o the value of $\Delta\eta$ is obtained by dividing $(\eta_i-\eta_o)$ over n (the number of steps in the η-direction).

For given $\Delta\xi$ and Δt the numerical procedure continues as follows. For each value of j (starting from $j=2$) equation (15) is applied with $i=2,3,\ldots$, and n to give $(n-1)$ equations in $(n-1)$ unknown values of θ. The matrix of coefficients of the resulting system of linear equations is a tridiagonal matrix and hence Thomas' method is used to obtain a numerical solution for the interior grid points (for each value of j). This procedure is repeated for all values of j from $j=2$ until $j=m$ to scan the whole mesh network. Equations (16) and (17) are used to obtain the values of θ on the two ξ-boundaries. Moreover, equation (18) or equation (19) is used to obtain the values of θ on the adiabatic boundary in cases 3.I and 3.O, respectively. The obtained values of θ at the present time step will then be considered as old values (superscripted θs) for the next time step and thus the whole process can be repeated until steady-state conditions are reached. Steady-state conditions mean that the obtained values of θ do not change with further increase in time.

The steady-state analytical solutions provided a check on the adequacy of the present computer code

and consequently on the obtained transient numerical results. The obtained numerical transient solutions were found to asymptotically approach (at considerably large values of the time t) the available steady-state solutions given by equation (14) and Table 1. None of the computer runs was allowed to stop before the obtained transient numerical results converge to the corresponding steady-state analytical solution with a maximum tolerance less than 1% (in the value of the local dimensionless temperature θ at any mesh point). On the other hand, a thorough numerical experimentation has been conducted to investigate the effect of mesh sizes on the obtained numerical results and the computer CPU time. For example, the obtained steady-state times for case 1.O with $N = 0.5$, $Q = 5$, $E = 0.5$ and $\Delta t = 10^{-3}$ corresponding to mesh sizes $m \times n = 20 \times 20$, 25×25, 30×30, 20×40, 35×35 and 35×40 are, respectively, 0.512, 0.511, 0.511, 0.507, 0.509 and 0.509. The corresponding computer CPU times (using WF 77 Sys D) are, respectively, 63.35, 98.90, 142.52, 128.07, and more than 180 in the last two cases. Similarly, the obtained steady-state times for the same values of N, Q, E and Δt in case 1.I for mesh sizes $m \times n = 20 \times 15$, 20×20, 20×25, 20×30, 20×35, 25×25, 40×20, 30×30 and 40×35 are, respectively, 0.514, 0.507, 0.504, 0.501, 0.500, 0.505, 0.500, 0.503 and 0.501. It might be worth mentioning that time steps as low as 10^{-5} were used in some cases (at the expense of the computer execution time). However, for the sake of unification in comparisons all the results presented in the present paper have been obtained using $m \times n = 20 \times 20$ and $\Delta t = 10^{-3}$.

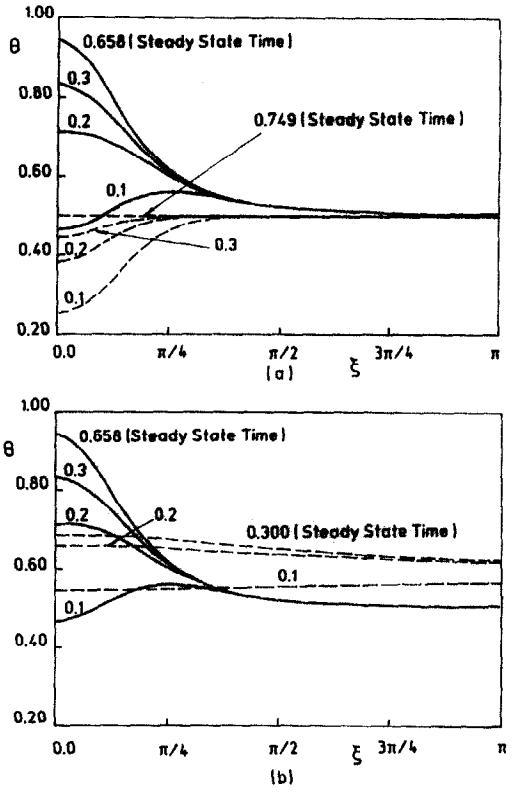

Fig. 2. (a) Effect of Q on transient temperature distribution at $\eta = \eta^*$ in case 1.I, $N = 0.5$, $E = 0.8$, ---- $Q = 0$, —— $Q = 5$; (b) effect of eccentricity on transient temperature distribution at $\eta = \eta^*$ in case 1.I, $N = 0.5$, $Q = 5$, - - - $E = 0.1$, —— $E = 0.8$.

RESULTS AND DISCUSSION

For case 1.I and a given E ($E = 0.8$) in an annulus of $N = 0.5$, Fig. 2(a) shows the variation with time of the dimensionless temperature on an intermediate surface having $\eta = \eta^* = (\eta_i + \eta_o)/2$ for two values of Q, namely, $Q = 0$ and 5. For either value of Q and a given ξ, the temperature of this surface increases with time until it reaches the steady-state value (at $t_s = 0.749$ and 0.658 for $Q = 0$ and 5, respectively). The figure shows that, for any value of Q, the narrow side of the annulus ($\xi \to \pi$) reaches the steady-state conditions much faster than the wide side ($\xi \to 0$). This is attributed to the larger heat storage capacity of the wide side compared to that of the narrow side. On the other hand, for given time and ξ the temperature value with internal heat generation is as expected, larger than its corresponding value without internal heat generation ($Q = 0$).

The effect of eccentricity on the transient response of the temperature of the system is clarified in Fig. 2(b). For case 1.I and a given Q ($Q = 5$) in an annulus of $N = 0.5$, this figure gives the variation with time of the dimensionless temperature on the intermediate surface of $\eta = \eta^* = (\eta_i + \eta_o)/2$ for two values of E, namely, $E = 0.1$ and $E = 0.8$. As can be seen from this figure, the eccentricity has a prominent effect on the transient temperature distribution. For a given time (t), as the value of E increases the temperature distribution on the surface of a given η becomes more dependent on ξ. In a concentric annulus ($E = 0$) in both cases 1.I and 1.O, the isothermal lines, without or with internal heat generation, are concentric circles, i.e. the temperature is independent of the angular coordinate. However, as the annulus deviates from the concentric situation the temperature in the wide side ($\xi \to 0$) becomes higher than that in the narrow side ($\xi \to \pi$). This is due to the larger internal heat generated in the wide side of the annulus since this side has more solid material per unit length than the narrow side.

Figure 3(a) shows the transient temperature distribution on the insulated boundary of an annulus of radius ratio 0.5 and dimensionless eccentricity 0.7 under thermal boundary conditions 3.I and 3.O without internal heat generation. Due to the presence of an insulated boundary, steady-state can only be achieved under these conditions when the solid temperature becomes uniform and equals the temperature of the heated boundary (i.e. dimensionless temperature $\theta_s = 1$ everywhere). As can be seen from Fig. 3(a), as the time elapses the temperature of the insulated surface (and similarly that of the internal solid material)

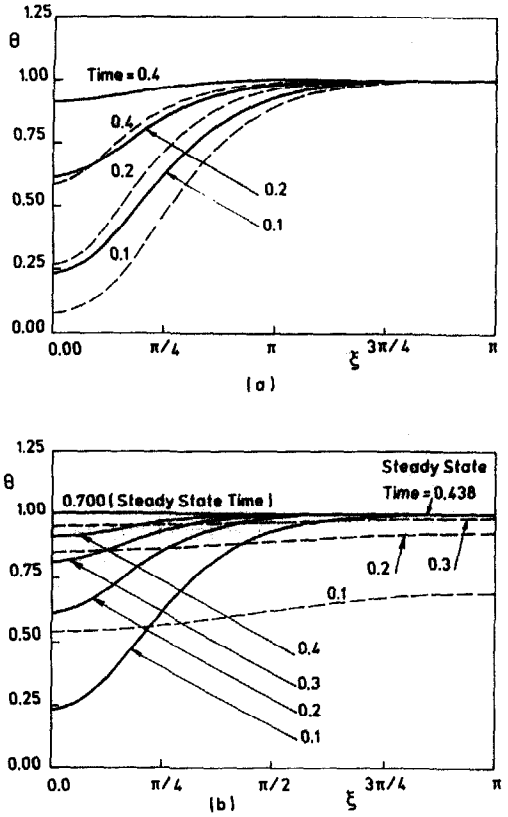

Fig. 3. (a) Effect of boundary conditions on temperature distribution on insulated wall, $N = 0.5$, $E = 0.7$, $Q = 0$, – – – case 3.I, —— case 3.O; (b) transient temperature distribution on the inner insulated wall temperature in case 3.O, $N = 0.5$, $Q = 0$, – – – – $E = 0.1$, ——$E = 0.7$.

increases and approaches asymptotically the aforesaid unity value. However, the narrow-side of the annulus reaches such steady-state conditions faster than the wide-side. Therefore, the process of increasing the temperature towards equalization at steady-state conditions occurs not only by diffusion of heat in the radially-like (η) direction (from the heat transfer boundary to the insulated surface) but also in the circumferential ξ-direction (from the narrow-side to the wide-side of the annulus). This latter mechanism of conduction heat transfer has a longer path than the former (which is the only mechanism in a concentric case) and hence it can be anticipated that eccentricity, as will be shown later, would increase the time needed to reach steady-state conditions. For given time and ξ, Fig. 3(a) shows that the temperature under thermal boundary conditions 3.O is higher than that under thermal boundary conditions 3.I. Moreover, the system reaches steady-state conditions in case 3.O faster than in case 3.I. These are attributed to the larger heat transfer surface area in case 3.O than in case 3.I. Moreover, reaching steady-state more quickly for case 3.O is also probably due to the surface over which the temperature is kept constant at the steady-state value $\theta = 1$ (i.e. there is much more material at $\theta = 1$).

To clarify the effect of eccentricity, Figs. 3(b) and 4(a) give the time-variation of the insulated (inner) wall temperature for two values of eccentricity, namely, $E = 0.1$ and $E = 0.7$, in an annulus of $N = 0.5$ under thermal conditions 3.O without and with internal heat generation, respectively. Both figures show that increasing the value of E makes the temperature more dependent on the ξ-coordinate. Without internal heat generation ($Q = 0$), the ξ-direction diffusion of heat is always from the narrow side ($\xi \to \pi$) to the wide side ($\xi \to 0$), as shown in Fig. 3(b). However, with internal heat generation ($Q \neq 0$) Fig. 4(a) shows that at large values of time the ξ-direction diffusion of heat reverses its direction and becomes from the large side to the narrow side of the annulus. This is attributed to there being more material per unit length on this side and hence the increase in the temperature of the solid in the wide side as a result of internal heat generation. Figure 4(b) focuses on the pronounced effect of eccentricity on the insulated wall temperature. This figure gives the steady-state temperature distribution on the outer wall of an annulus of $N = 0.5$ under thermal conditions 3.I for a value of $Q = 5$. The figure clearly shows that increasing the value of E causes an increase in the wall temperature on the wide side and a decrease in this temperature on the narrow side.

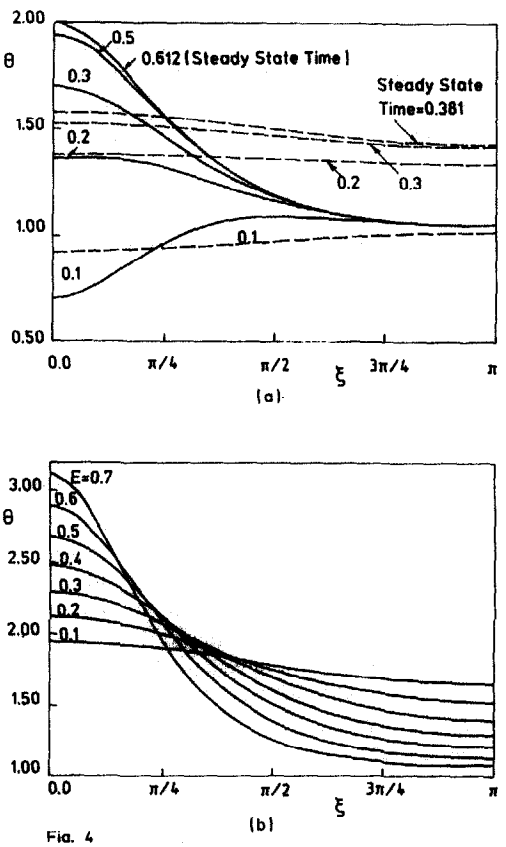

Fig. 4. (a) Transient temperature distribution on the inner insulated wall in case 3.O, $N = 0.5$, $Q = 5$, – – – – $E = 0.1$, ——$E = 0.7$; (b) steady-state temperature distribution on the outer insulated wall in case 3.I for various eccentricities, $N = 0.5$, $Q = 5$.

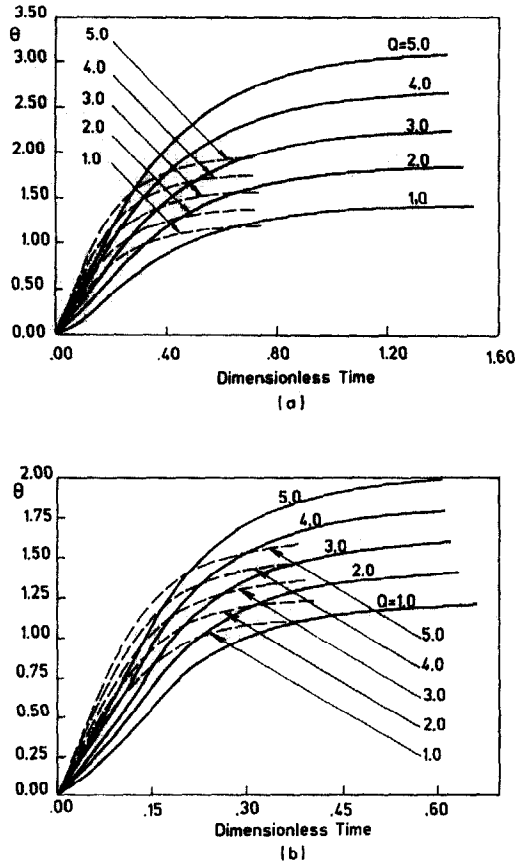

Fig. 5. (a) Variation of maximum temperature on the outer insulated wall in case 3.I, $\xi = 0$, $N = 0.5$, ---- $E = 0.1$, ——$E = 0.7$; (b) variation of maximum temperature on the inner insulated wall in case 3.O, $\xi = 0$, $N = 0.5$, ---- $E = 0.1$, ——$E = 0.7$.

Engineers are not frequently concerned with the details of the temperature field but only with maximum temperature and the time required to reach steady-state conditions. From the previous presented results it is clear that for given time, E and Q, the maximum solid temperature in both cases 3.I and 3.O would occur on the insulated wall at $\xi = 0$. Figures 5(a) and (b) give for cases 3.I and 3.O, respectively, the variation of such maximum temperature with time at two different eccentricity values in an annulus of $N = 0.5$ for various values of Q. On the other hand, Figs. 6(a) and (b) give the time required to reach steady-state conditions under the four thermal boundary conditions investigated. It is worth mentioning that the computer runs for any of the curves shown in these two figures (i.e. a given E) were made using the same η and ξ mesh sizes so that the order of numerical error magnitude would be the same for all values of Q. As can be seen from these two figures, for a given E, increasing the value of Q generally decreases slightly the time needed to reach the steady-state conditions. On the other hand, for a given Q, increasing the value of E increases prominently the time required to achieve steady-state. The time required to achieve steady-state conditions is of great value to thermal and control engineers.

CONCLUSIONS

Transient conduction heat transfer with uniform rate of internal heat generation has been numerically investigated in infinitely long eccentric hollow cylinders under the fundamental boundary conditions of the first and third types. In all cases considered, either with or without internal heat generation, the obtained results show that eccentricity has a pronounced effect on the transient thermal response of the system. Eccentricity creates a diffusion of heat in the second (ξ or circumferential) direction from the narrow side of the solid annulus to its wide side; this diffusion decreases with time. On the other hand, the internal heat generation creates also a ξ-diffusion of heat but in the opposite direction (from the wide side of the annulus to its narrow side); this diffusion increases with time. Finally, variation of the time required to reach steady-state conditions with eccentricity and internal heat generation has been given for all cases considered.

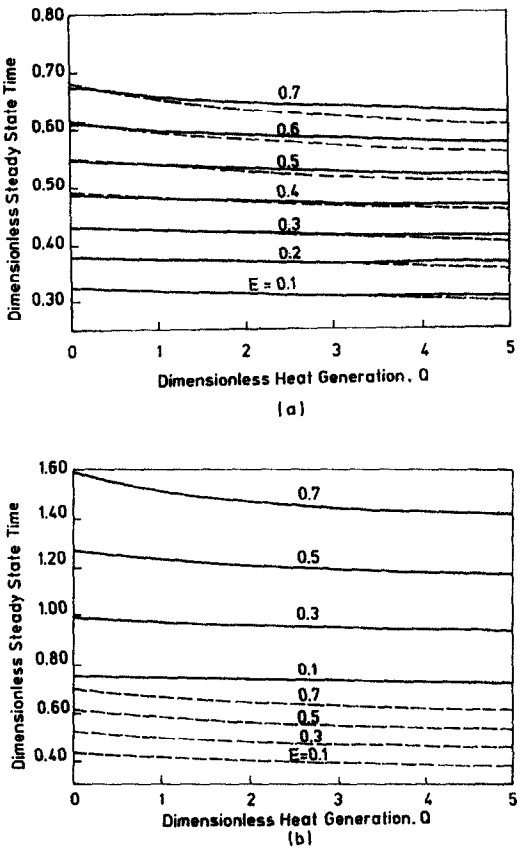

Fig. 6. (a) Steady-state time against heat generation for various eccentricities, $N = 0.5$, ---- case 1.I, —— case 3.O; (b) steady-state time against heat generation for various eccentricities, $N = 0.5$, ---- case 3.I, —— case 3.O.

Acknowledgement—The support of King Fahd University of Petroleum & Minerals to conduct this investigation is gratefully acknowledged.

REFERENCES

1. R. S. Abdulhadi and J. C. Chato, Combined natural and forced convective cooling of underground electric cables, *IEEE Trans. Power Apparatus Systems* **PAS-96,** 1–8 (1977).
2. M. A. I. El-Shaarawi and A. Sarhan, Developing laminar free convection in an open-ended vertical annulus with a rotating inner cylinder, *J. Heat Transfer* **103,** 552–558 (1981).
3. M. A. I. El-Shaarawi and M. A. Al-Nimr, Fully developed laminar natural convection in open-ended vertical concentric annuli, *Int. J. Heat Mass Transfer* **33,** 1873–1884 (1990).
4. M. N. Ozisik, *Heat Conduction*, p. 96. Wiley, New York, (1980).
5. W. C. Reynolds, R. E. Lundberg and P. A. McCuen, Heat transfer in annular passages. General formulation of the problem for arbitrarily prescribed wall temperatures or heat fluxes, *Int. J. Heat Mass Transfer* **6,** 483–493 (1963).
6. R. E. Lundberg, W. C. Reynolds and W. M. Kays, Heat transfer in annular passages. Hydrodynamically developed laminar flow with arbitrarily prescribed wall temperatures or heat fluxes, *Int. J. Heat Mass Transfer* **6,** 495–529 (1963).
7. M. L. Trombetta, Laminar forced convection in eccentric annuli, *Int. J. Heat Mass Transfer* **14,** 1161–1173 (1971).
8. M. R. El-Saden, Heat conduction in an eccentrically hollow, infinitely long cylinder with internal heat generation, *J. Heat Transfer* **83,** 510–512 (1961).
9. E. R. G. Eckert and R. M. Drake, *Analysis of Heat and Mass Transfer*, pp. 99–106. McGraw-Hill, New York (1972).
10. R. F. DeFelice and H. H. Bau, Conductive heat transfer between eccentric cylinders with boundary conditions of the third kind, *J. Heat Transfer* **105,** 678–680 (1983).
11. I. A. Ioffe, A problem of transient heat conduction in a semibounded body with an internal cylindrical heat source, *J. Engng Phys.* **23,** 1051–1054 (1972).
12. R. Thiyagarajan and M. M. Yovanovich, Thermal resistance of a buried cylinder with constant flux boundary condition, *J. Heat Transfer* **96,** 249–250 (1974).
13. H. H. Bau and S. S. Sadhal, Heat losses from a fluid flowing in a buried pipe, *Int. J. Heat Mass Transfer* **25,** 1621–1629 (1982).
14. W. W. Martin, and S. S. Sadhal, Bounds on transient temperature distribution due to a buried cylindrical heat source, *Int. J. Heat Transfer* **21,** 783–789 (1978).
15. P. Moon and D. E. Spencer, *Field Theory Handbook*, (2nd Edn), p. 53. Springer, Berlin (1971).
16. P. M. Morse and H. Feshback, *Methods of Theoretical Physics*—II, pp. 1214–1215. McGraw-Hill, New York (1953).